Journal of
Synchrotron
Radiation

ISSN 0909-0495

Received 18 March 2011
Accepted 13 May 2011

# Asynchronous sampling for ultrafast experiments with low momentum compaction at the ANKA ring

**Shyjumon Ibrahimkutty,[a] Daniel Issenmann,[a] Stefan Schleef,[a] Anke-Susanne Müller,[a,b] Yves-Laurent Mathis,[a] Biliana Gasharova,[a] Erhart Huttel,[a] Ralph Steininger,[a] Jörg Göttlicher,[a] Tilo Baumbach,[a,b] Albrecht Bartels,[c] Christof Janke[c] and Anton Plech[a,c]***

[a]Institute for Synchrotron Radiation, Karlsruhe Institute of Technology, PO Box 3640, D-76021 Karlsruhe, Germany, [b]Laboratory for Application of Synchrotron Radiation, Karlsruhe Institute of Technology, PO Box 3640, D-76021 Karlsruhe, Germany, and [c]Center for Applied Photonics, University of Konstanz, Universitätsstrasse 10, D-78457 Konstanz, Germany.
E-mail: anton.plech@kit.edu

A high-repetition-rate pump–probe experiment is presented, based on the asynchronous sampling approach. The low-$\alpha$ mode at the synchrotron ANKA can be used for a time resolution down to the picosecond limit for the time-domain sampling of the coherent THz emission as well as for hard X-ray pump–probe experiments, which probe structural dynamics in the condensed phase. It is shown that a synchronization of better than 1 ps is achieved, and examples of phonon dynamics of semiconductors are presented.



**Keywords: picosecond time resolution; laser excitation; electro-optical sampling; coherent phonons.**

## 1. Introduction

By reducing the so-called momentum compaction factor $\alpha$ (thus called low-$\alpha$ optics), electron pulses as short as 500 fs (root mean square) can be achieved. The electromagnetic emission of these short pulses occurs in a coherent wave up to frequencies considerably above 1 THz. An efficient mechanism for the emission of coherent and also for incoherent radiation is the synchrotron radiation emission at the entry point of the electron beam into the field at the magnetic dipoles of the ring. This so-called edge radiation is used for a number of experiments at infrared beamlines around the world. ANKA, BESSY (Berlin, Germany) and the SLS (Villigen, Switzerland) regularly offer beam time in low-$\alpha$ mode for users.

Within the coherent regime all electrons in the pulse radiate in phase, which has several important consequences: the emitted power scales with the square of the pulse charge while incoherent emission only scales linearly (Carr *et al.*, 2002). A strong gain in power is expected for the coherent emission with typical bunch charges being in the range of 100 pC (Abo-Bakr *et al.*, 2002; Karantzoulis *et al.*, 2008). At ANKA a coherent flux of 0.2 mW is extracted in a spectral region from 0.2 to 2 THz (Müller *et al.*, 2008*a*) at the diagnostics port of the IR1 beamline. A detailed discussion of the ring parameters at which pulse compression can be achieved can be found by Hiller *et al.* (2010). In particular, the electron energy is lowered at ANKA from 2.5 to 1.3 or 1.6 GeV to reduce $\alpha$. Another consequence of the coherence is the phase-stable emission relative to the pulse position. This means that the oscillation phase of the electrical field is fixed relative to the pulse envelope (carrier-envelope stability).

At the same time the ultrashort pulses will emit incoherent radiation up to the hard X-ray range with the same time duration. A time resolution in the picosecond range represents a particularly valuable tool for structural studies, for example of solids. Compared with the typical pulse length at a synchrotron of about 100 ps (full width at half-maximum, FWHM) this improved time resolution allows structural dynamics to be addressed beyond the thermalization limit. The thermal equilibration time of the electron and phonon system is typically of some 1–10 ps. Being able to resolve this time scale will enable us to investigate different kinds of coherent processes, such as coherent phonon excitation or non-thermal structure formation.

In conventional time-resolved experiments a femtosecond oscillator of typically 80 MHz repetition rate is synchronized to the bunch clock of synchrotrons by a piezoelectric feedback loop (Schotte *et al.*, 2002; Plech *et al.*, 2009*a*). A typical short-term stability of some 3–5 ps is achieved routinely. This jitter is clearly too large to resolve coherent THz radiation and also for the envisaged pump–probe experiments. Very recently large efforts have been devoted to synchronizing lasers to the free-electron laser FLASH, achieving a sub-100 fs precision by using a master oscillator to drive the photo-gun of the injector (Loehl *et al.*, 2008). At the synchrotron, in contrast, a

continuous dynamic feedback from the ring current has to be used to correct for drifts in repetition rate and for dynamic excitations with the synchrotron frequency.

In this communication we show that, by using a high-frequency femtosecond oscillator and establishing a feedback control at the 2.5 GHz overtone of the repetition frequency, a high precision of the synchronization can be achieved. By additionally introducing the asynchronous sampling technique, a very sensitive detection of the electro-optical (EO) modulation owing to the THz field from the synchrotron is possible, as well as a time-resolved experiment in the X-ray range.

## 2. Set-up

The goal of the set-up is to use the full repetition rate of 500 MHz in order to obtain a high signal-to-noise ratio for the THz-field sampling and for detection of laser-induced lattice changes in the photo-excited samples. The peak brightness in the X-ray regime suffers from the reduction of the electron energy from 2.5 GeV to 1.3 or 1.6 GeV and a lower ring current. This makes a low-repetition-rate experiment unfavorable. The central demand for a high temporal stability of the laser source is achieved by using a Ti:sapphire oscillator (Gigaoptics, 2 nJ pulse energy, 800 nm center wavelength, 50 fs pulse length) at the synchrotron repetition rate. Its frequency is stabilized by means of a fast feedback loop to the synchrotron by using the pick-up from a stripline detector in the ring. A set of two piezo-actuated cavity mirrors provide a long stroke adjustment on the time scale of seconds and a fast feedback with a 8 kHz frequency cut-off. The fast feedback reacts on the fast modulations and dynamics of the electron beam.

We employed the recently developed asynchronous sampling in order to avoid the usage of mechanical or electronic delay lines with their sensitivity to drifts and the difficulties in defining the temporal overlap. In the optical regime this ASOPS (asynchronous optical sampling) has been demonstrated as an extremely sensitive tool for femtosecond spectroscopy and THz sampling (Bartels *et al.*, 2006, 2007; Plech *et al.*, 2007). Inspired by this we call our approach the optical-X-ray sampling ASOXS.

The working principle is that both sources of radiation are detuned in frequency by a very small amount, which shifts the mutual time delay from pulse pair to pulse pair by a tiny increment, such that a femto- to picosecond delay between the pulses is mapped onto a nano- to microsecond time scale of the detection system. Therefore a detector fast enough to resolve the beat frequency is required, which translates into the modulation of the ultrafast delay. In practice a detuning of 10 kHz is used, which, at a pulse spacing of 2 ns, translates to a delay shift of 40 fs or equivalently 1 ps/50 ns record length between subsequent pulse pairs. This is easily resolved by optical detectors and X-ray avalanche diodes.

For the feedback the fifth overtone of the signal from a laser pick-up photodiode is frequency shifted by an analog mixer and then compared with the related pick-up signal from the synchrotron. The error signal is transduced *via* a PI (proportional-integral) controller to the high-voltage amplifiers of the piezo-actuators. A trigger signal is generated from the beat of the two input frequencies and used to start the data acquisition interval.

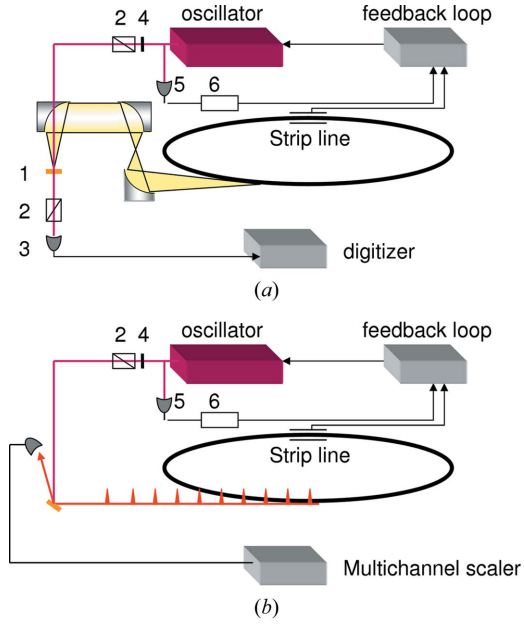


**Figure 1**
Schematic layout of the THz sampling (*a*) and the ASOXS set-up for the asynchronous X-ray probe set-up. In the THz set-up (*a*) the IR beamline part is strongly simplified. The laser beam is focused onto the ZnTe crystal (1) between two almost crossed polarizers (2) and a half-wave plate (4) and registered by a photo-receiver (3). A second photo-receiver (5) monitors the laser pulse frequency, which is shifted by a frequency mixer (6) and compared with the synchrotron pulse frequency from the strip line. The phase difference acts as error signal for the feedback loop, which actuates two cavity mirrors. The same loop stabilizes the laser for the ASOXS set-up (*b*), while the laser excites the sample, which is probed by the X-ray pulses and registered in an APD.

The exact coincidence of both sources at the sample, with respect to the EO crystal, is arbitrary relative to the trigger event, but can be tuned by an electronic phase shifter or adapted cable lengths. The jitter for this trigger is lower than 100 ns at the end of a 100 µs real-time delay span. This amounts to less than 2 ps at maximum. The coincidence point is then directly taken from the time-resolved data. This procedure is common to almost all laser X-ray techniques, as cross-correlators are difficult to implement.

A scheme of the set-up is shown in Fig. 1 for both cases of THz sampling and time-resolved X-ray scattering.

## 3. THz emission

The THz electrical field can be sampled by an optical laser pulse with duration much shorter than the THz frequency, given that both are synchronized to better than the period. The method of detection is the EO effect, by which the polarization of the laser is slightly rotated within a crystal (zinc telluride, ZnTe) when applying an electrical field, in this case from the THz pulse. Thus a direct time-domain trace of the

electric field oscillation can be reconstructed. Earlier experiments have used Fourier-transform infrared spectroscopy setups to determine the field autocorrelation function, which, however, does not give the full phase information. The EO approach is therefore well suited as a diagnostics tool for the emission and consequently for the electron charge distribution and dynamics of the stored electron bunches.

In order to probe the optical rotation through a detectable intensity variation, a ZnTe crystal is placed between a polarizer/analyzer combination for the femtosecond laser beam (Bartels *et al.*, 2006) at almost crossed orientation. As a result any rotation of the laser polarization in the crystal results in an intensity modulation at the optical detector. As the polarizers are not fully crossed, the transmitted intensity is finite and the modulation can be both positive and negative. It mirrors the electric field polarization. A quarter-wave plate removes any static circular component of the optics. Orthogonal polarizations of laser and THz field are used at the ⟨110⟩ surface of the ZnTe crystal (0.5 mm thickness) (Planken *et al.*, 2001). The linearity of response to the electrical field is sufficient for the detected intensity changes of $10^{-5}$ (Casalbuoni *et al.*, 2008).

The THz pulses are extracted at the direct diagnostics port of the IR1 beamline at ANKA (Müller *et al.*, 2008*a*). The beam is guided *via* refocusing gold-coated mirrors and a diamond vacuum window to the experiment with a 6 mm *z*-cut quartz window at the exit. There the radiation enters ambient atmosphere and is focused onto the ZnTe crystal by an off-axis paraboloid mirror (50 mm diameter, 75 mm focal length) to a diameter of about 2 mm. The laser beam is overlapped with this spot by focusing with a 100 mm lens through a coaxial hole in the paraboloid. A photo-receiver with a bandwidth of 100 MHz plus a 200 MHz digitizer (GaGe Applied) finally record the time-resolved intensity of the probe laser beam.

Fig. 2 displays the change in laser intensity after passing through the Glan-Laser prism analyzer. For this curve a number of $10^5$ individual traces were recorded (Plech *et al.*, 2009*b*). This is equivalent to a total integration time of 100 s.

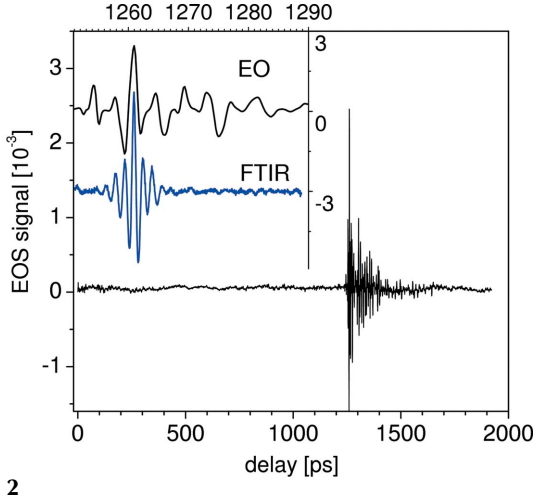


**Figure 2**
Electro-optical AC signal within the ZnTe crystal within the complete 2 ns pulse-to-pulse separation. The inset shows a magnification of the prompt signal together with a comparison with the FTIR delay trace.

The noise level is at $10^{-7}$ of the incoming laser intensity and displays a modulation of $3 \times 10^{-5}$.

A large oscillating signal is recorded at a given (arbitrary) delay relative to the trigger, which is generated by the beat frequency between laser and synchrotron radiation. The first oscillation is followed by a number of subsequent ringings. Looking closer at the strongest cycle one recognizes the picosecond variation of the field in accordance with the pulse length at this synchrotron setting. The subsequent oscillations have a slightly longer period. A comparison is shown in the inset with the intensity trace of the FTIR spectrometer, whose delay scan can be interpreted as an autocorrelation function of the electrical field. It is of the same time scale.

The ideal emission from a symmetric electron pulse should be a single cycle of the electrical field (Sannibale *et al.*, 2004; Müller *et al.*, 2008*b*), which is not the case here. Several effects contribute to the deviation. Firstly, the THz pulse propagates in air for a short distance of about 60 cm after exiting the quartz viewport. The absorption in humid atmosphere adds absorption bands from water vapor, some of which are located at around 0.57, 0.76 and 0.96 THz. These bands are responsible for subsequent oscillations after the first field pulse according to the Fourier theorem at the resonance frequency. Secondly, the THz propagation can no longer be described by geometrical optics if the numerical aperture is small. The beamline has been designed and optimized for IR extraction. However, in the THz region, diffraction effects and reflections on the beam tubes cause a distortion of the wavefront. This is seen as multiple oscillating signals and delayed emission that are recorded for some hundred picoseconds. A similar observation has been reported by an intensity-based detection with high time resolution (Hübers *et al.*, 2005) at the synchrotron BESSY II. Finally, wake fields in the ring chamber are responsible for bunch-to-bunch feedback in multibunch filling modes. These fields (or whispering-gallery modes) could contribute to the signal pattern. This latter effect is a matter of current investigations.

A comparison of the Fourier transform of the time-domain signal with a FTIR spectrum that has been acquired at the same time is shown in Fig. 3. A Bruker IFS 66v/S FTIR (Bruker Optics) was used with a 0.05 mm mylar beam splitter and a silicon bolometer as detector. The spectral content of both curves is quite similar, which proves that the synchronization of the laser is indeed precise enough to resolve about 1.4 THz, which in turn translates to a precision better than 0.7 ps. The fine structure of the spectrum will be governed by the above-mentioned contributions. Thus the THz spectra allow us to follow the bunch modification with tuning the beam optics. The EO sampling even shows stronger contributions below 0.5 THz than the FTIR curve, which is due to an artifact of the performance of the beam splitter in the Fourier-transform spectrometer at low frequency.

In Fig. 4 the spectral content of the THz emission is shown for two accelerating voltages of the high-frequency (HF) cavities. When the voltage is raised from 150 kV to 400 kV per cavity the bunches are compressed longitudinally, and thus become shorter. As a consequence the cut-off for coherent

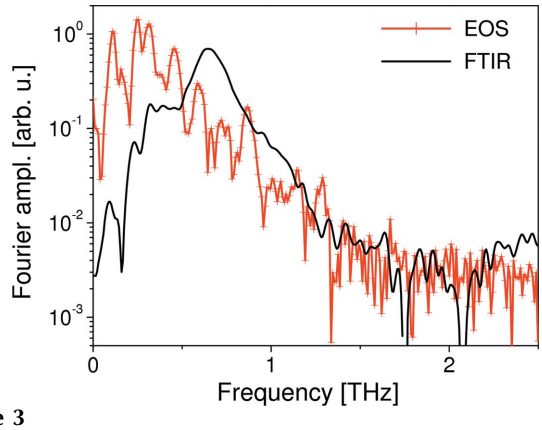


**Figure 3**
Fourier transform of the electro-optical signal (EOS) within 15 ps around the main maximum in comparison with a parallel spectral measurement of the radiation in a Fourier transform IR spectrometer (FTIR).

emission (which is solely detected here) shifts to shorter wavelength or equivalently to a higher frequency. During a stepwise increase of the high voltage one can see a transition in the emitted intensity, which correlates with the so-called bursting threshold. At this threshold the pulses start to develop a dynamic fine structure owing to the interaction with the wake fields. As the pulse envelope starts to deviate from a Gaussian charge distribution the THz emission is enhanced. For the higher voltage the spectrum extends to above 1 THz, while for the lowest voltage the spectral power decays to below 0.5 THz.

The EO sampling can therefore deliver complementary information on the coherent emission to detection schemes with spectroscopy means of bolometric detection (Müller *et al.*, 2009*b*; Probst *et al.*, 2011).

The role of the averaging process on the signal shape may be questioned when taking into account the beam dynamics. Therefore we have performed a stepwise reduction of the number of averages from $10^5$ down to a single trace. A single trace can be recorded within one trigger interval. This still

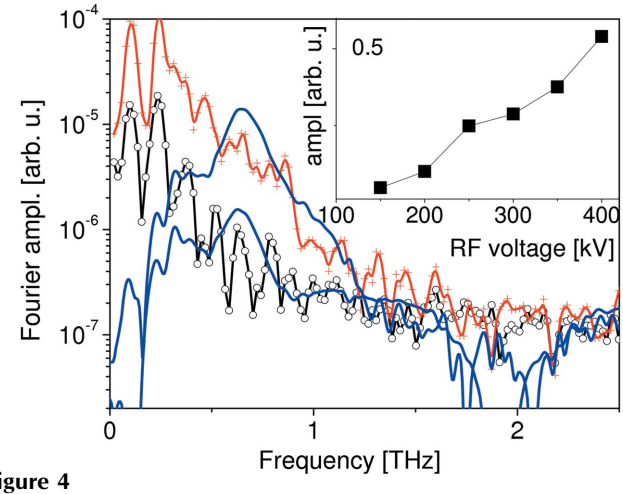


**Figure 4**
Fourier spectra of the electro-optical signal as in Fig. 3, but recorded at different accelerating voltages in the HF cavities of the synchrotron. The inset shows the time domain amplitude of the electro-optical signal as a function of the accelerating voltage.

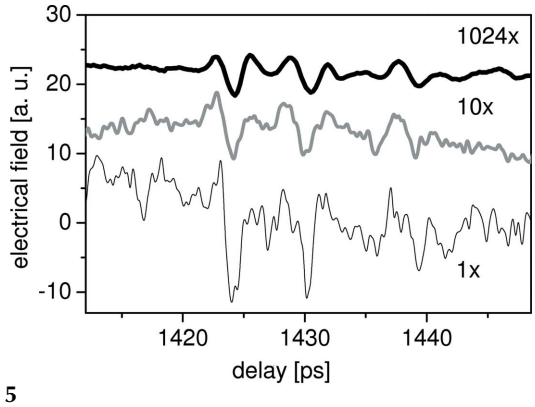


**Figure 5**
Electro-optical signal around the pulse arrival delay for a different number of sampling averages from a single 100 µs trace to a 1024-fold average. The curves are displaced for clarity.

means that a complete series of laser pulses samples subsequent THz pulses at an increasing delay, but any given pulse is only sampled once. Assuming that the bursting dynamics is variable on a sub-millisecond time scale, this single trace should reflect the instantaneous emission. We find (within the limits of noise level) that the transient THz signal is preserved in shape even during such a single sweep. Only the amplitude of the electrical field is about twice the averaged signal. Already after averaging ten traces the signal is of the same amplitude as the average shown in Fig. 5. As a result the signal is influenced by the averaging procedure to a certain extent, for example by longitudinal oscillations of the pulses in the HF field. These oscillations are, in any case, not detrimental to detecting the THz field.

Therefore the coherent part of the THz radiation, which is phase stable to the laser pulses, can be recorded by the EO sampling with high sensitivity. Averaging reduces the instantaneous emission signal, *e.g.* from bursting bunches, but preserves the overall spectral content. Therefore this method can be a valuable tool for following electron beam dynamics either by sampling the THz emission (*i.e.* in the far-field) (Müller *et al.*, 2010) or in the near-field close to the electron beam (Berden *et al.*, 2006; Steffen *et al.*, 2009).

## 4. Asynchronous sampling for time-resolved X-ray diffraction

In low-$\alpha$ mode the bunch length can be reduced to the picosecond scale, which is attractive for ultrafast structural investigations. Such experiments follow the pump–probe scheme, whereby a laser pulse acts as excitation source and creates a non-equilibrium state in the sample. Subsequently this state decays with characteristic time scales and intermediate states, which give deeper insight in the interactions that determine the material properties.

The X-ray experiment can be performed with the same scheme as shown earlier (see also Fig. 1). While the laser pulses excite the sample at the 500 MHz repetition rate, the X-ray pulses probe the structural changes asynchronously. Two critical issues have to be solved for this purpose. First,

an X-ray detector with a sufficient time resolution has to be used to follow the asynchronous sampling. Here we employ an avalanche photodiode detector (APD) (Baron, 1994) (Cyberstar, FMB Oxford), which shows an excellent time resolution of less than 5 ns (FWHM) and consequently also allows for high count rates in the photon-counting mode. The counts are sorted according to their arrival time in a multi-channel scaler with 4 ns bin width (Nanoharp, Picoquant). Second, the pulses of the laser are necessarily quite weak owing to the high repetition rate. Therefore a strong focusing has to be applied in order to achieve a fluence on the sample, which is sufficient for significant amplitudes of structural changes. In coherent phonon motion, for example, the fluence for achieving large changes of the Bragg scattering of semiconductor crystals is typically in the range 1–5 mJ cm$^{-2}$ (Reis *et al.*, 2001; Bargheer *et al.*, 2004; Sondhauss *et al.*, 2005). The laser fluence is maximized by focusing both laser and X-ray beams down to a 35 µm (FWHM) spot size.

The whole set-up is accommodated at the SUL-X beamline at ANKA, which is optimized for microfocus absorption spectroscopy and scattering (see Fig. 6). A wiggler source delivers $5 \times 10^8$ (1.6 GeV) or $1.8 \times 10^8$ photons s$^{-1}$ (100 mA)$^{-1}$ (1.3 GeV) in low-$\alpha$ mode [magnetic gap at 20 mm, Si(111) bandwidth] at 5.5 keV. The X-rays are focused by a Kirkpatrick–Baez (KB) mirror pair onto the laser-irradiated spot. A slit at an intermediate focus position allows the spot size to be reduced further. A miniature diffractometer is added onto the multi-axis sample stage to allow for diffraction in vertical geometry. For this demonstration of ASOXS we investigated a (111) germanium and a (100) GaAs crystal surface, where the laser absorption depth is close to the X-ray extinction depth for the Bragg reflections. The synchrotron settings were 1.6 GeV, 200 kV per cavity, four trains of 30 bunches each filled in the ring, and a synchrotron frequency of 7.3 kHz.

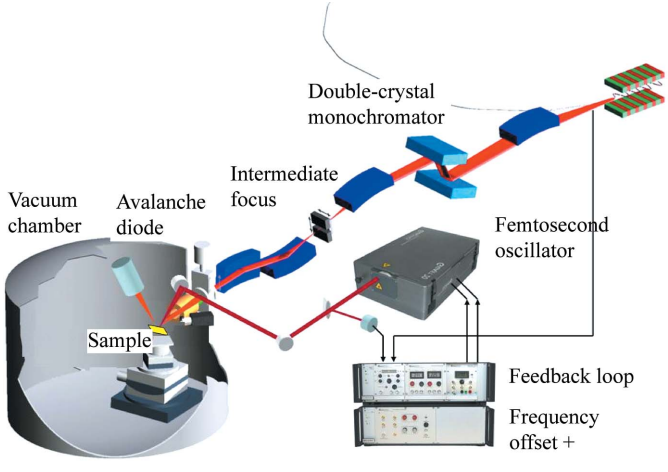


**Figure 6**
Design of the time-resolved set-up at SUL-X within the vacuum chamber. An independent miniature goniometer for a vertical scattering plane together with the APD detector arm. A motorized lens stage provides the means for aligning the laser focus relative to the X-ray focus. The laser is coupled in *via* the vacuum windows.

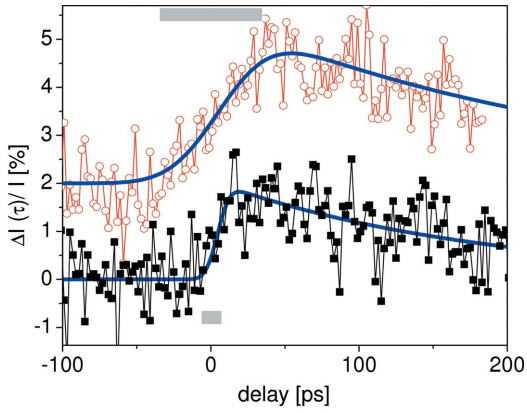


**Figure 7**
Time-resolved intensity change at the expansion side of the Ge(111) Bragg reflection as a function of delay between laser and X-ray pulses. The open symbols represent data taken during normal optics of the synchrotron (shifted upwards for clarity), while data with full symbols are acquired during low-$\alpha$ operation. The lines are fits with a sigmoidal rise and exponential decay and the gray bars mark the 10 to 90% signal change.

The X-ray extinction depth for the Ge(111) reflection, 0.6 µm, is closest to the laser absorption depth, thus the excited and probed volume should match best. In Fig. 7 a typical trace of the change of scattered intensity as a function of delay is shown for normal operation and for the low-$\alpha$ optics. An X-ray scattering of about $6 \times 10^7$ photons s$^{-1}$ was used at the maximum of the Bragg reflection (35 µm spot size at an intermediate focus of 0.15 × 0.15 mm). As the incidence angle was detuned to the low-angle side from the Bragg position, an intensity increase reflects the excitation of acoustic phonon modes with a fast expansion of the lattice. It is clearly seen that the rise time of the signal shortens from 28 ps (r.m.s.) to 6.5 ps (r.m.s.) in low-$\alpha$ mode. This time scale is in agreement with the calculated bunch lengths of 5.5 ps from the used compaction factor (Hiller *et al.*, 2010). In Lindenberg *et al.* (2000) the lattice excitation through femtosecond laser irradiation is described by two mechanisms: a thermally induced lattice expansion through the electron–phonon coupling followed by a rarefaction wave propagating into the bulk, and a quasi-instantaneous displacive force through hot carriers. While the thermal pathway is slow owing to the finite electron–phonon coupling time and the sound propagation, the second mechanism is faster than the present pulse lengths and causes coherent phonon motion. At an angular shift of 0.002 Å$^{-1}$ one would expect a phonon period of about 11 ps, which should result in a rise time of the scattering change of some 5 ps (10–90%). Thus the observed rise time is still governed by the X-ray pulse length and oscillations are washed out. The decay on the longer time scale reflects the propagation of the expansion into the bulk.

The accuracy of the signal is dominated by the photon statistics. The reflectivity at 0.002 Å$^{-1}$ deviation from the (111) peak was only 5%, which results in 3000 photons per time bin per second. At integration times of 40 s the Poisson noise can be predicted to be 0.3%. The observed noise level is about 0.5% and thus close to the predicted one.

A further compression of the X-ray pulses is possible, but the optimum has to be found for the transversal size of the electron beam with possible wiggler gap settings and the reduction of the lifetime on the one hand and reduction of momentum compaction factor on the other.

The change in diffracted intensity amounts to only 2.5%. This corresponds to a Bragg angle change of $7.4 \times 10^{-6}$ and is equivalent to a temperature rise of 0.9 K assuming thermal expansion. This demonstrates that even small shifts or intensity changes of the peaks can be resolved.

A full map of the transient intensity change has been derived for the GaAs (400) reflection by detuning the incident angle stepwise relative to the Bragg angle and recording the ASOXS signal at each position. Shown in Fig. 8 is a color-coded map of the relative change of scattering intensity. At the low-angle side a transient intensity increase indicates the expansional motion subsequent to the excitation. This expansion relaxes back within hundreds of picoseconds owing to heat diffusion and phonon propagation. The excitation of coherent acoustic phonon modes will additionally cause a modulation of the intensity at a frequency which increases with the shift from the Bragg position. This behaviour reflects the linear dispersion of the acoustic phonon branch close to the zone center.

The data show a clear increase of the steepness of lattice expansion to the left side with distance from the Bragg peak center at 54.05°. The subsequent modulation is, however, smeared out. This smearing is caused by several effects. First, the KB focusing optics introduce a beam divergence, which reduces the angular resolution. Second, the spot sizes of laser and X-rays are comparable, which introduces a gradient of excitation amplitude across the X-ray footprint. Therefore the quasi-static shift of the Bragg reflection (owing to the laser heat deposition) is broadened and mixes phonon-induced modulations of different wavevectors. While the beam angular acceptance was set to about 0.014°, the broadening amounts to another 0.02°. One should note that the quasi-static shift of the reflection reaches 0.075°, which is equivalent to a temperature rise of 175 K.

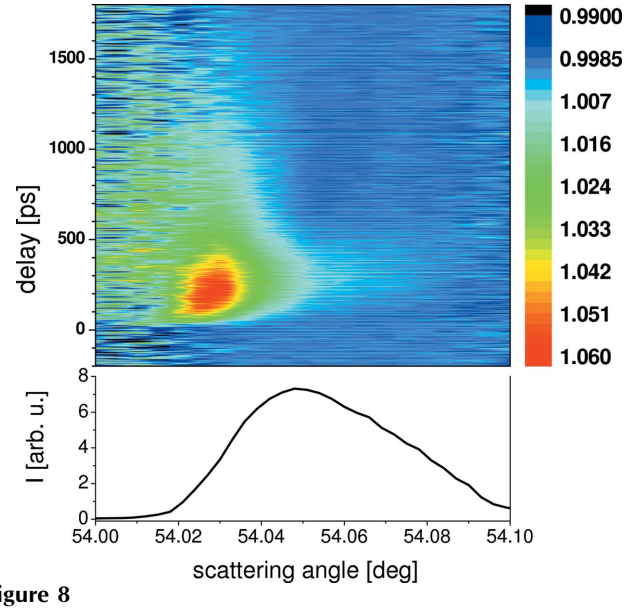


**Figure 8**
False-color map of of the intensity change of the scattering close to the (400) Bragg reflection of a GaAs surface. The Bragg profile is shown in the lower graph.

The typical total exposure time for the map shown in Fig. 8 is in the range of less than 1 h, which covers 40 angular settings and the complete time span of 2000 ps. A detector slit or analyzer was not used for the shown data. The data show that ASOXS is capable of deriving complete maps of scattering intensity changes down to a confidence level of 0.5% for the given parameters. This is equivalent to a temperature change (or phonon amplitude) lower than 0.2 K per laser shot.

## 5. Conclusions and outlook

In conclusion, a reliable method for detecting coherent synchrotron radiation in low-$\alpha$ mode at ANKA is described by phase-locking a femtosecond high-repetition laser to the synchrotron repetition rate. The electrical field is detected in amplitude and phase by the electro-optical effect. This information may allow for a more detailed diagnostics of the electron pulses stored in the ring. The THz radiation can be used in time-domain spectroscopy as has been demonstrated for laboratory-based THz sources. The complex dielectric function in this spectral region can be obtained without the use of the Kramers–Kronig relation.

The synchronization of the laser to the synchrotron emission is better than 0.7 ps as seen by the resolution of the coherent electrical field oscillation of the THz field for frequencies above 1 THz.

The main goal of the set-up was to perform time-resolved X-ray scattering on crystalline samples with high time resolution. We could show that the acoustic phonon motion in semiconductor crystals can be addressed within a reasonable exposure time both in delay and angular dependence. At the realised set-up the resolution is limited by the angular acceptance of the focused X-ray beam and the non-uniformity of the laser excitation amplitude across the X-ray footprint. The latter can be relaxed at the expense of overall excitation amplitude. An analyzer crystal or a narrow slit at the detector position could increase the sensitivity further. One important aspect for the development of the set-up will be the use of an APD array, which will take advantage of the beam divergence to cover the entire peak region with one setting of the incidence angle. Thus a parallel detection will increase the counting statistics and resolution. Structural signals other than peak shifts from acoustic modes will be less sensitive on the beam divergence, for example optical phonon modes or spectroscopic signals. We expect that a more brilliant X-ray source, such as a superconducting undulator, will increase the signal-to-noise contrast.

The ASOXS method can be of interest when studying small-amplitude motion through reversible excitation, such as phonon motion, in order to determine elastic properties, *e.g.* near phase transitions (Dougherty *et al.*, 1994; Plech *et al.*, 2007). Nanostructured crystalline systems show modulated

phonon signatures, such as breathing modes or zone folding (Bartels *et al.*, 2007), which can be studied with atomic resolution by this approach (Bartels *et al.*, 1999; Bargheer *et al.*, 2004; Sondhauss *et al.*, 2005).

Finally, the asynchronous sampling may be applicable for other high-repetition-rate machines, where a very precise detection of small transient scattering changes is required. A repetition rate down to a few MHz may still take advantage of the ASOXS set-up, for example at linear accelerators (TBONE; Müller *et al.*, 2009*a*) or energy-recovering machines (Abo-Bakr *et al.*, 2009).

We would like to thank T. Dekorsy, R. Weigel, R. Rossmanith and N. Hiller for valuable input. Assistance with the operating and tuning of the machine in low-$\alpha$ mode by P. Wesolowski is acknowledged. The work is supported by the DFG *via* grants and a Heisenberg Fellowship.

## References

Abo-Bakr, M., Anders, W., Kamps, T., Knobloch, J., Kuske, B., Kugeler, O., Matveenko, A., Meseck, A., Neumann, A. & Quast, T. (2009). *Proceedings of the 14th International Conference on RF Superconductivity (SRF2009)*, Berlin, Germany. TUPPO017.

Abo-Bakr, M., Feikes, J., Holldack, K., Wüstefeld, G. & Hübers, H.-W. (2002). *Phys. Rev. Lett.* **88**, 254801.

Bargheer, M., Zhavoronkov, N., Gritsai, Y., Woo, J. C., Kim, D. S., Woerner, M. & Elsaesser, T. (2004). *Science*, **306**, 1771–1773.

Baron, A. Q. R. (1994). *Nucl. Instrum. Methods Phys. Res. A*, **353**, 665–667.

Bartels, A., Cerna, R., Kistner, C., Thoma, A., Hudert, F., Janke, C. & Dekorsy, T. (2007). *Rev. Sci. Instrum.* **78**, 035107.

Bartels, A., Dekorsy, T., Kurz, H. & Köhler, K. (1999). *Phys. Rev. Lett.* **82**, 1044–1047.

Bartels, A., Hudert, F., Janke, C., Dekorsy, T. & Köhler, K. (2006). *Appl. Phys. Lett.* **88**, 041117.

Berden, G., van der Meer, A., Jamison, S. P., Steffen, B., Knabbe, E.-A., Schmidt, B., Schmüser, P., MacLeod, A., Phillips, P. J. & Gillespie, W. (2006). *Proceedings of the Tenth European Particle Accelerator Conference (EPAC'06)*, Edinburgh, Scotland. TUPCH027.

Carr, G. L., Martin, M. C., McKinney, W. R., Jordan, K., Neil, G. R. & Williams, G. P. (2002). *Nature (London)*, **420**, 153.

Casalbuoni, S., Schlarb, H., Schmidt, B., Schmüser, P., Steffen, B. & Winter, A. (2008). *Phys. Rev. STAB*, **11**, 072802.

Dougherty, T. P., Wiederrecht, G. P., Nelson, K. A., Garrett, M. H., Jenssen, H. P. & Ward, C. (1994). *Phys. Rev. B*, **50**, 8996–9019.

Hiller, N., Hillenbrand, S., Hofmann, A., Huttel, E., Judin, V., Kehrer, B., Klein, M., Marsching, S., Müller, A.-S., Plech, A., Smale, N., Sonnad, K. & Tavares, P. (2010). *Proceedings of the First International Particle Accelerator Conference (IPAC'10)*, Kyoto, Japan. WEPEA020.

Hübers, H.-W., Semenov, A., Holldack, K., Schade, U., Wüstefeld, G. & Gol'tsman, G. (2005). *Appl. Phys. Lett.* **87**, 184103.

Karantzoulis, E., Penco, G., Perucchi, A., Ortolani, M. & Lupi, S. (2008). *Proceedings of the 11th European Particle Accelerator Conference (EPAC08)*, Genoa, Italy, p. 2043.

Lindenberg, A. M., Kang, I., Johnson, S. L., Missalla, T., Heimann, P. A., Chang, Z., Larsson, J., Bucksbaum, P. H., Kapteyn, H. C., Padmore, H. A., Lee, R. W., Wark, J. S. & Falcone, R. W. (2000). *Phys. Rev. Lett.* **84**, 111–114.

Loehl, F., Arsov, V., Hacker, K., Lorbeer, B., Ludwig, F., Matthiesen, K., Schlarb, H., Schmidt, B., Winter, A., Schulz, S., Zemella, J., Szewinski, J. & Jalmuzna, W. (2008). *Proceedings of the 11th European Particle Accelerator Conference (EPAC08)*, Genoa, Italy, p. 3360.

Müller, A.-S., Baumbach, T., Casalbuoni, S., Gasharova, B., Hagelstein, M., Huttel, E., Mathis, Y.-L., Moss, D., Plech, A., Rossmanith, R., Bründermann, E., Havenith, M., Hillenbrand, S. & Sonnad, K. (2009*a*). *Proceedings of the 23rd Particle Accelerator Conference (PAC09)*, Vancouver, BC, Canada. TU5RFP028.

Müller, A.-S., Birkel, I., Casalbuoni, S., Gasharova, B., Huttel, E., Mathis, Y.-L., Moss, D. A., Smale, N. J., Wesolowski, P., Bründermann, E., Bueckle, T. & Klein, M. (2008*a*). *Proceedings of the 11th European Particle Accelerator Conference (EPAC08)*, Genoa, Italy, p. 2091.

Müller, A.-S., Birkel, I., Huttel, E., Mathis, Y.-L., Smale, N., Hübers, H.-W., Semenov, A., Feikes, J., von Hartrott, M., Wüstefeld, G., Klein, R., Müller, R., Ulm, G., Bründermann, E., Bückle, T., Fitterer, M., Hillenbrand, S., Hiller, N., Hofmann, A., Judin, V., Klein, M., Marsching, S. & Sonnad, K. (2009*b*). *Proceedings of the 23rd Particle Accelerator Conference (PAC09)*, Vancouver, BC, Canada. TU5RFP027.

Müller, A.-S., Casalbuoni, S., Fitterer, M., Huttel, E., Mathis, Y.-L. & Schmelling, M. (2008*b*). *Proceedings of the 11th European Particle Accelerator Conference (EPAC08)*, Genoa, Italy, p. 2094.

Müller, F., Steffen, B., Schlott, V. & Chevtsov, P. (2010). *Proceedings of the 2010 Beam Instrumentation Workshop (BIW10)*, Santa Fe, NM, USA. TUPD31.

Planken, P. C., Nienhuys, H.-K., Bakker, H. & Wenckebach, T. (2001). *J. Opt. Soc. Am. B*, **18**, 313–317.

Plech, A., Boneberg, J. & Leiderer, P. (2009*a*). *Laser Phot. Rev.* **3**, 435–451.

Plech, A., Casalbuoni, S., Gasharova, B., Huttel, E., Mathis, Y.-L., Müller, A.-S., Sonnad, K., Bartels, A. & Weigel, R. (2009*b*). *Proceedings of the 23rd Particle Accelerator Conference (PAC09)*, Vancouver, BC, Canada. TU5RFP026.

Plech, A., Cerna, R., Kotaidis, V., Hudert, F., Bartels, A. & Dekorsy, T. (2007). *Nano Lett.* **7**, 1026–1031.

Probst, P., Scheuring, A., Hofherr, M., Rall, D., Wünsch, S., Ilin, K., Siegel, M., Semenov, A., Pohl, A., Hübers, H.-W., Judin, V., Müller, A.-S., Hoehl, A., Müller, R. & Ulm, G. (2011). *Appl. Phys. Lett.* **98**, 043504.

Reis, D. A., DeCamp, M. F., Bucksbaum, P. H., Clarke, R., Dufresne, E., Hertlein, M., Merlin, R., Falcone, R., Kapteyn, H., Murnane, M. M., Larsson, J., Missalla, T. & Wark, J. S. (2001). *Phys. Rev. Lett.* **86**, 3072–3075.

Sannibale, F., Byrd, J. M., Loftsdóttir, A., Venturini, M., Abo-Bakr, M., Feikes, J., Holldack, K., Kuske, P., Wüstefeld, G., Hübers, H.-W. & Warnock, R. (2004). *Phys. Rev. Lett.* **93**, 094801.

Schotte, F., Techert, S., Anfinrud, P. A., Srajer, V., Moffat, K. & Wulff, M. (2002). *Third-Generation Hard X-ray Synchrotron Radiation Sources.* Berlin: John Wiley and Sons.

Sondhauss, P., Larsson, J., Harbst, M., Naylor, G. A., Plech, A., Scheidt, K., Synnergren, O., Wulff, M. & Wark, J. S. (2005). *Phys. Rev. Lett.* **94**, 125509.

Steffen, B., Schlott, V. & Müller, F. (2009). *Proceedings of the 9th European Workshop on Beam Diagnostics and Instrumentation for Particle Accelerators (DIPAC09)*, Basel, Switzerland. TUPB42.